IEEE Access
Multidisciplinary | Rapid Review | Open Access Journal

Received December 17, 2018, accepted December 28, 2018, date of publication January 17, 2019, date of current version February 12, 2019.

Digital Object Identifier 10.1109/ACCESS.2019.2893619

Channel Prediction for Millimeter Wave MIMO-OFDM Communications in Rapidly Time-Varying Frequency-Selective Fading Channels

CHANGWEI LV[1], JIA-CHIN LIN[2], (Senior Member, IEEE), AND ZHAOCHENG YANG[3,4]

[1]Shenzhen Institute of Information Technology, Shenzhen 518172, China
[2]Department of Communication Engineering, National Central University, Taoyuan 32001, Taiwan
[3]College of Information Engineering, Shenzhen University, Shenzhen 518067, China
[4]The Guangdong Key Laboratory of Intelligent Information Processing, College of Information Engineering, Shenzhen University, Shenzhen 518060, China

Corresponding author: Zhaocheng Yang (yangzhaocheng@szu.edu.cn)

This work was supported in part by National Natural Science Foundation of China under Grant 61771317, and in part by the Natural Science Foundation of SZU under Grant 827-000236.

ABSTRACT The millimeter wave (mmWave) multiple-input multiple-output (MIMO) orthogonal frequency division multiplexing (OFDM) systems communicate at the extremely high-frequency band. In the extremely high band, the channel state information (CSI) from channel estimation will be outdated quickly, and herein, seriously degrading the system performance. In this paper, we focus on the channel prediction to obtain prior CSI in mmWave MIMO-OFDM systems. First, the mmWave MIMO-OFDM channel is categorized and represented in four domains: the array-frequency, array-time, angle-frequency, as well as angle-time. Then, for the above four domains, we investigate the effects of the channel representations on channel prediction, and analyze the mean-squared error performance as well as the computational complexity of the investigated prediction methods. We derive that the angle-time-domain prediction method achieves higher accuracy than the other three prediction techniques. In addition, we propose an enhanced angle-time-domain channel predictor by exploiting the spatial-time sparsity of the MIMO-OFDM channel to further improve the prediction accuracy. Finally, the simulation results confirm the statistical analysis and verify the superiority of the proposed predictors.

INDEX TERMS Channel prediction, channel representations, millimeter wave, sparse channel, MIMO-OFDM systems.

I. INTRODUCTION

Multi-input multi-output (MIMO) and orthogonal frequency division multiplexing (OFDM) are two key technologies to improve communications over a wireless channel [1]. With multiple transmit and multiple receive antennas, MIMO systems can obtain either a diversity gain or a multiplexing gain compared with the single-input single-output (SISO) systems [2]. Meanwhile, on wideband transmission, OFDM systems have a superior ability to mitigate inter-symbol interference (ISI) without the need of sophisticated equalization techniques compared with the single-carrier (SC) systems [3]. Recently, the millimeter wave (mmWave) communication is regarded as one of the most potential solutions for the exponentially expanding wireless data traffic in the future, due to the wide usable spectrum in the millimeter waveband [4], [5]. Almost all mobile communication systems today use spectrum in the range of 300 MHz-5 GHz, while the mmWave systems typically use frequencies at 6 GHz-100 GHz (although the wavelength of 6 GHz-30 GHz is actually in centimeter level) [6], [7]. The mmWave systems enable gigabit-per-second data rates to meet the future demands for mobile traffic by leveraging the abundant frequency spectrum resource. To compensate for huge pathloss of communication in mmWave bands, MIMO technique is fundamental for providing beamforming gain to ensure coverage of a serving cell [8]–[10]. To fully exploit the ultra-wideband communication resources of mmWave communication, OFDM method is necessary for communication systems to convert the frequency-selective fading channels into a parallel collection of frequency-flat sub-channels and

reducing ISI [7]. Therefore, the combination of mmWave, MIMO and OFDM has been considered as a promising technology for the wireless communication systems [11]–[13].

MmWave communication systems face several new design challenges as compared to the conventional lower-frequency counterparts [14], [15]. In particular, due to the significantly higher frequency used, mmWave channels usually suffer from much faster variation [16], [17], thus the mmWave channel coherent time maybe significantly reduced [18] and becomes shorter than the frame transmission time. There are at least two types of techniques seriously affected by the above challenge. The first type of technique is the coherent signal detection at receiver. In the coherent signal detection, accurate channel estimates are required at the receiver to achieve the symbol detection. Traditionally, channel estimation is usually obtained in a data-aided mode, where pilots known to the receiver are transmitted in each frame to enable the estimation method at each pilot position [19]. Then, the estimated CSI is used for the detection of data in the frame. However, the CSI acquisition based on channel estimation in mmWave MIMO-OFDM systems may provide outdated information, thus seriously degrade the signal detection performance. The other type of technique is the adaptive transmission. Adaptive transmission has been proposed to provide high throughput for many communication systems [20], and shown to play a key role in the choice of space-time algorithms, the use of adaptive modulation and coding, and the number of antennas employed at both ends of the radio link. Adaptive transmission invariably requires accurate CSI on the upcoming transmission frame. In the rapidly time-varying mmWave channels, the CSI obtained by channel estimation will be outdated soon, and can not satisfy the demand of adaptive transmission. In both circumstances, reliable channel prediction is necessary to forecast the channel variation [21].

Channel prediction techniques have been studied to effectively compensate for the outdated CSI in the scenario where the SISO SC systems work in flat fading channels [22]–[24]. Recently, the channel prediction concept has been extended to the MIMO-OFDM systems that operate in frequency-selective channels [25], [26]. Generally speaking, the MIMO-OFDM channel can be represented in two types: the former is related to the MIMO technique, and it is configured as in either array domain (ARD) or angle domain (AGD); the latter is related to the OFDM technique, and it is configured as in either frequency domain (FD) or time domain (TD). Therefore, the MIMO-OFDM channel can be represented in four combinatorial domains: the array-frequency domain (AR-FD), the array-time domain (AR-TD), the angle-frequency domain (AG-FD), and the angle-time domain (AG-TD). The channel estimation for the above channel representations in MIMO-OFDM systems have been addressed in [27]–[31]. However, the study in [27]–[31] did not extend to channel prediction. For the MIMO systems, the minimum mean-square-error (MMSE) or adaptive channel predictors are proposed in [26], [32], and [33], and a parametric-model-based channel prediction method is proposed in [34]. They all work on each pair of antennas in the ARD. For the OFDM systems, most of the existing predictors are realized on each subcarrier in the FD [35]–[37], while [38] proposes to predict the channel coefficients in the TD. For the MIMO-OFDM systems, the previously proposed prediction methods operate on each subcarrier in each antenna pair of MIMO-OFDM channel [18], [25], [26], [39]. Since channel vector is determined by the direction of arrival (DOA) information and the gain information, [40] and [41] propose a channel tracking method for mmWave massive MIMO systems, which operates the channel tracking in the angle domain by tracking the DOA and estimating its corresponding gain.

To the best of our knowledge, the existing papers did not consider to predict the mmWave channels in the combinatorial domains which are derived from the aforementioned two domain types, and also did not study the effects of the channel representations on the channel prediction, which will be our main focus in this paper. We first derive the channel prediction techniques in the AR-FD, the AR-TD, the AG-FD, and the AG-TD. The autoregressive (AR) model is employed to conduct prediction on each domain and then estimate the CSI according to the MMSE prediction assisted from a number of past estimates. Moreover, we study the effects of channel representation in MIMO-OFDM systems on channel prediction, and show the MSE performance of the proposed prediction methods. We verify that the TD and the AGD channel prediction are respectively more accurate than the FD and the ARD channel prediction. Furthermore, it is derived that the AG-TD prediction method is more accurate than the other three techniques. To improve the channel prediction performance in the AG-TD, we also propose an enhanced AG-TD prediction method, which exploits the sparse features of a realistic radio channel in both the AGD and the TD. The computational complexity comparisons of the four domain prediction methods are conducted, and show that the enhanced AG-TD reduces the computation a lot due to the exploitation of sparse features of channel. Simulation results are then used to confirm the analysis, and verify the effectiveness of the proposed prediction techniques.

The remainder of this paper is organized as follows. Section II describes the mmWave MIMO-OFDM system model. Section III briefly studies the MIMO-OFDM channel representations and their relationships, as well as the statistics. Section IV derives the mmWave channel prediction techniques in the individual domains. Section V compares performance among different predictors, including the MSE performance, computational complexity, and some further discussions. Section VI proposes the enhanced AG-TD prediction method. Section VII illustrates the performance evaluations, while Section VIII is the conclusion.

II. mmWave MIMO-OFDM SYSTEM MODEL

Fig. 1 shows a typical mmWave MIMO-OFDM system model. We consider a MIMO system deploying uniform

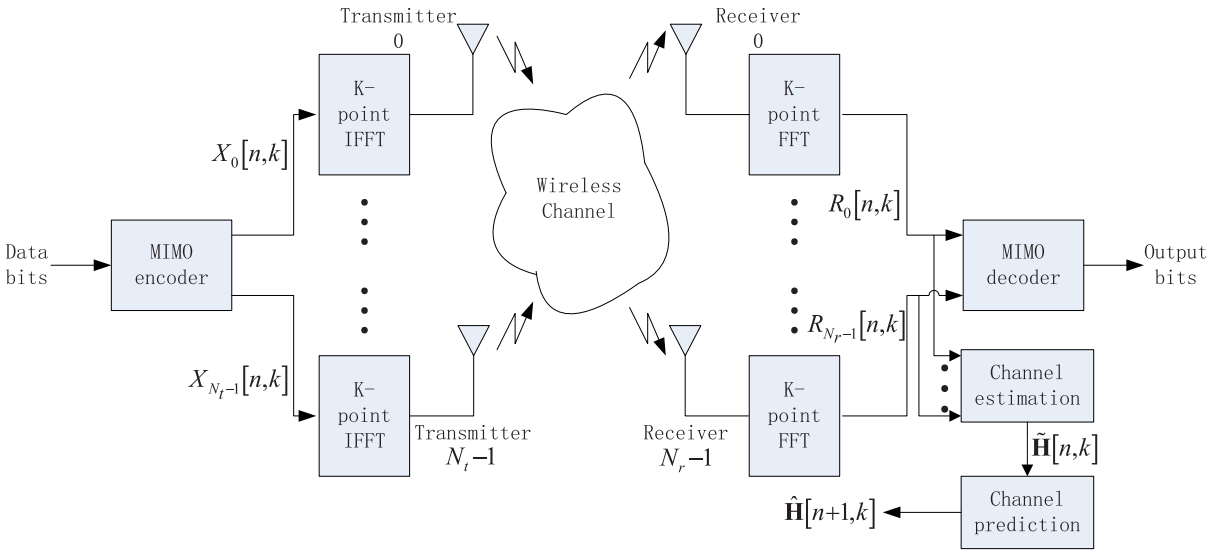

FIGURE 1. MIMO-OFDM system model.

linear arrays (ULA) geometry at both ends with N_r receive and N_t transmit antennas. Therefore, the MIMO channel consists of $N_r \times N_t$ propagation sub-channels. As the mmWave channel is usually wideband and frequency-selective, an OFDM technique with K sub-carriers is combined with the MIMO technique to turn the frequency-selective fading channel into a set of flat fading channels. At time n, the input data block is mapped into N_t complex constellation sequences $\{X_v[n,0], X_v[n,1], \cdots, X_v[n,K-1]\}$, for $v = 0, 1, \cdots, N_t - 1$. Then, the OFDM uses an inverse discrete Fourier transform (IDFT) to modulate the transmit signal and a DFT to demodulate the received signal. With proper cyclic prefix (CP) length L_{cp}, the received signal after DFT at receiver u can be given by [1]

$$R_u[n,k] = \sum_{v=0}^{N_t-1} H_{uv}[n,k] X_v[n,k] + Z_u[n,k], \quad (1)$$

where $H_{uv}[n,k]$ is the channel frequency response from the vth transmitter to the uth receiver on the subcarrier k of the OFDM block at time n, and $Z_u[n,k]$ is the additive white Gaussian noise (AWGN). For each OFDM subcarrier k, columnwisely arrange $R_u[n,k]$, $u = 0, 1, \cdots, N_r - 1$ into a vector $\boldsymbol{r}[n,k]$, and then (1) can be rewritten in the matrix form of

$$\boldsymbol{r}[n,k] = \boldsymbol{H}[n,k]\boldsymbol{x}[n,k] + \boldsymbol{z}[n,k], \quad (2)$$

where

$$\begin{aligned}\boldsymbol{r}[n,k] &= \left[R_0[n,k]\ R_1[n,k]\ \cdots\ R_{N_r-1}[n,k]\right]^T \\ \boldsymbol{x}[n,k] &= \left[X_0[n,k]\ X_1[n,k]\ \cdots\ X_{N_t-1}[n,k]\right]^T \\ \boldsymbol{z}[n,k] &= \left[Z_0[n,k]\ Z_1[n,k]\ \cdots\ Z_{N_r-1}[n,k]\right]^T, \end{aligned} \quad (3)$$

and the superscript "T" denotes the transpose operator. $\boldsymbol{H}[n,k]$ represents the channel for the kth subcarrier of the nth OFDM symbol, as shown in (4), at the top of the next page. $\boldsymbol{H}[n,k]$ is the so called AR-FD representation of MIMO-OFDM channel.

The channel estimation followed by the channel prediction is also shown in Fig. 1. To predict the future channel weights, the channel estimators in [1], [43], and [44] should be conducted at first. For the channel estimation, it is necessary to insert the pilot symbols. Note that in order to perform channel prediction, the channel sampling rate (pilot density) should be higher than the Nyquist rate which is twice of the maximum Doppler frequency occurring with the wireless channel. With pilot symbols, the estimates of corresponding channel can be obtained. In this paper, we focus on the channel prediction technique and specify no particular channel estimation method. We just give out the estimation result at the pilot position directly as follows

$$\tilde{H}_{uv}[n,k] = H_{uv}[n,k] + N_{uv}[n,k], \quad (5)$$

where $N_{uv}[n,k]$ is the estimation noise assumed to be a zero mean Gaussian random variable with variance σ^2. Here, we define the estimation SNR as

$$\mathrm{SNR}_{estm} = E\left\{\|\boldsymbol{H}[n,k]\|^2\right\} \Big/ \sigma^2.$$

III. mmWave MIMO-OFDM CHANNEL CHARACTERISTICS

Before investigating channel prediction for MmWave MIMO-OFDM systems, we describe the channel representations in four domains, and emphasize the relationships among the four representations. In this section, we also investigate the statistics of the four channel representations.

A. CHANNEL REPRESENTATIONS AND THEIR RELATIONSHIPS

The mmWave MIMO-OFDM channel is usually introduced in the AR-TD, and thus we first describe the AR-TD channel

$$\boldsymbol{H}[n,k]=\begin{bmatrix} H_{00}[n,k] & H_{01}[n,k] & \cdots & H_{0(N_t-1)}[n,k] \\ H_{10}[n,k] & H_{11}[n,k] & \cdots & H_{1(N_t-1)}[n,k] \\ \vdots & \vdots & \ddots & \vdots \\ H_{(N_r-1)0}[n,k] & H_{(N_r-1)1}[n,k] & \cdots & H_{(N_r-1)(N_t-1)}[n,k] \end{bmatrix}. \tag{4}$$

representation. The MIMO channel impulse response (CIR) can be extended from the common SISO channel model [27], and the complex baseband representation of a SISO CIR can be given as

$$c(t,\tau)=\sum_k c_k(t)\,\delta(\tau-\tau_k), \tag{6}$$

where τ_k is the delay of the kth channel tap, and $c_k(t)$ is the corresponding tap gain. Due to the motion of the receivers, the kth channel tap gain $c_k(t)$ can be modeled as a sum of L_k complex sinusoids as

$$c_k(t)=\sum_{l=0}^{L_k-1}\alpha_{k,l}e^{jw_{k,l}t}, \tag{7}$$

where $\alpha_{k,l}$ is the scattering coefficient of the lth sinusoid in tap k, $w_{k,l}$ is the corresponding Doppler frequency. Then, the SISO channel can be extended to the MIMO channel by adding the spatial dimension as [27]

$$\boldsymbol{h}(t,\tau)=\sum_k \boldsymbol{C}_k(t)\,\delta(\tau-\tau_k), \tag{8}$$

where $\boldsymbol{C}_k(t)$ is the kth tap of MIMO channel, given as

$$\boldsymbol{C}_k(t)=\sum_{l=0}^{L_k-1}\boldsymbol{e}_r\left(\Omega_{k,l}^r\right)\alpha_{k,l}\sqrt{N_rN_t}e^{jw_{k,l}t}\boldsymbol{e}_t^H\left(\Omega_{k,l}^t\right), \tag{9}$$

the superscript "H" denotes the Hermitian transpose operater, and $\boldsymbol{e}_r\left(\Omega_{k,l}^r\right)$ and $\boldsymbol{e}_t\left(\Omega_{k,l}^t\right)$ are the array steering vectors for the receive and transmit antennas, respectively. $\boldsymbol{e}_r\left(\Omega_{k,l}^r\right)$ and $\boldsymbol{e}_t\left(\Omega_{k,l}^t\right)$ can be expressed as

$$\begin{aligned}\boldsymbol{e}_r\left(\Omega_{k,l}^r\right)&=\frac{1}{\sqrt{N_r}}\left[1,e^{j2\pi\Delta_r\Omega_{k,l}^r},\cdots,e^{j2\pi(N_r-1)\Delta_r\Omega_{k,l}^r}\right]^T\\ \boldsymbol{e}_t\left(\Omega_{k,l}^t\right)&=\frac{1}{\sqrt{N_t}}\left[1,e^{j2\pi\Delta_t\Omega_{k,l}^t},\cdots,e^{j2\pi(N_t-1)\Delta_t\Omega_{k,l}^t}\right]^T,\end{aligned} \tag{10}$$

where Δ_r is the separation distance between adjacent receive antennas normalized by λ_c, and λ_c is the wave length; $\Omega_{k,l}^r=\sin\varphi_{k,l}^r$, and $\varphi_{k,l}^r$ is the DOA of sinusoid l in channel tap k at the receiver; Δ_t is the separation distance between adjacent transmit antennas normalized by λ_c; $\Omega_{k,l}^t=\sin\varphi_{k,l}^t$, and $\varphi_{k,l}^t$ is the direction of departure (DOD).

For the OFDM system with symbol period T_s and subcarrier spacing Δf, the discrete-time channel impulse response can be obtained by sampling from $\boldsymbol{h}(t,\tau)$, and is given as $\boldsymbol{h}[n,l]$, with its element $h_{uv}[n,l]=h_{uv}\left(nT_s,l\big/(\Delta fK)\right)$ being the lth channel tap at the nth OFDM symbol from the vth transmitter to the uth receiver. Then, $\boldsymbol{h}[n,l]$'s, for $l=0,1,\cdots,L_t-1$ are the AR-TD representation of MIMO-OFDM channel, where L_t is the number of channel taps. In the receiver, by taking the DFT of the AR-TD channel representation, we can obtain the AR-FD channel representation in (4) as

$$H_{uv}[n,k]=\frac{1}{\sqrt{K}}\sum_{l=0}^{L_t-1}h_{uv}[n,l]\,e^{-j2\pi kl/K}. \tag{11}$$

(11) transforms the AR-TD channel representation into the AR-FD representation by using DFT operation, and herein the inverse transformation can be conducted using the IDFT operation.

According to [27] and [30], the AG-FD channel representation can be related to the AR-FD domain channel as

$$\boldsymbol{H}^a[n,k]=\boldsymbol{U}_r^H\boldsymbol{H}[n,k]\,\boldsymbol{U}_t, \tag{12}$$

where the superscript "a" denotes the angle-domain variables, $\boldsymbol{U}_r$ and $\boldsymbol{U}_t$ are the $N_r\times N_r$ and $N_t\times N_t$ unitary matrices respectively, and their (k,l) th entries are

$$\begin{aligned}&\frac{1}{\sqrt{N_r}}\exp\left(-\frac{j2\pi kl}{N_r}\right),\quad k,l=0,1,\cdots,N_r-1,\\ &\frac{1}{\sqrt{N_t}}\exp\left(-\frac{j2\pi kl}{N_t}\right),\quad k,l=0,1,\cdots,N_t-1,\end{aligned} \tag{13}$$

respectively. Hence, the transformation matrices $\boldsymbol{U}_r$ and $\boldsymbol{U}_t$ are unitary DFT matrices in this case, and they divide the AR-FD channel $\boldsymbol{H}[n,k]$ into N_r receive angular regions and N_t transmit angular regions, respectively. The entry of AG-FD channel, $H_{\alpha\beta}^a[n,k]$, represents the channel gain from the βth transmit angular bin to the αth receive angular bin. Equation (12) transforms the AR-FD representation into AG-FD representation via a two-dimensional Fourier transformation. Similarly, we can transform the AR-TD channel representation into AG-TD representation as

$$\boldsymbol{h}^a[n,l]=\boldsymbol{U}_r^H\boldsymbol{h}[n,l]\,\boldsymbol{U}_t. \tag{14}$$

where its element $h_{\alpha\beta}^a[n,l]$ is the lth channel tap at the nth OFDM symbol from the βth transmit angular bin to the αth receive angular bin.

For clarity, the relationships among the four channel representations are concluded as follows. On one hand, the OFDM technique employs DFT in the receiver to transform the TD channel into FD, and thus we can establish the frequency-time relationship of channel through DFT and IDFT [38], [42]. On the other hand, the MIMO technique extends the radio channel into space, for which we can abstract the ARD model into AGD model in terms of spatially resolvable

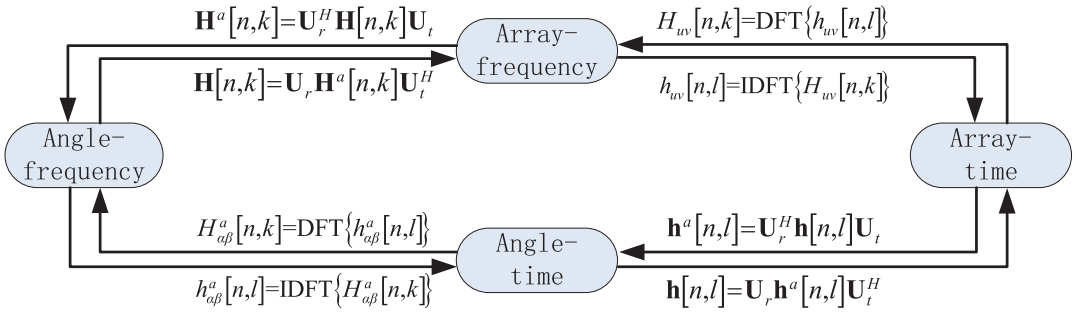

FIGURE 2. Relationships among the channel representations.

paths [27], [28]. The details of the relationships are shown in Fig. 2.

B. CHANNEL STATISTICS

The channel taps with different delays are often assumed to be wide sense stationary (WSS), independent, and narrowband complex processes. Meanwhile, in each channel tap, different physical paths (sinusoids) contribute to different AGD bins, and thus the channel coefficients in different AGD bins can be assumed to be spatially uncorrelated [27]. Therefore, the AG-TD channel correlation function can be expressed as

$$\begin{aligned} &r_{h^a}[\Delta n,\Delta\alpha,\Delta\beta,\Delta l] \\ &\quad=E\left\{h^a_{\alpha\beta}[n,l]\left(h^a_{\alpha'\beta'}[n',l']\right)^*\right\} \\ &\quad=r_{h^a_{\alpha\beta,l}}[\Delta n]\,\delta[\Delta\alpha]\,\delta[\Delta\beta]\,\delta[\Delta l], \end{aligned} \tag{15}$$

where $\Delta n = n - n'$, $\Delta\alpha = \alpha - \alpha'$, $\Delta\beta = \beta - \beta'$, $\Delta l = l - l'$, and $r_{h^a_{\alpha\beta,l}}[\Delta n]$ is the temporal correlation for the lth channel tap from the βth transmit angular bin to the αth receive angular bin.

Based on the AG-TD channel correlation in (15) and the relationships shown in Fig 2, we can respectively derive the channel correlations in the AG-FD, the AR-TD, and the AR-FD as follows:

$$\begin{aligned} &r_{H^a}[\Delta n,\Delta\alpha,\Delta\beta,\Delta k] \\ &=E\left\{H^a_{\alpha\beta}[n,k]\left(H^a_{\alpha'\beta'}[n',k']\right)^*\right\} \\ &=E\left\{\frac{1}{\sqrt{K}}\sum_{l=0}^{K-1}h^a_{\alpha\beta}[n,l]\,e^{-j2\pi\frac{kl}{K}}\right. \\ &\qquad\left.\times\left(\frac{1}{\sqrt{K}}\sum_{l'=0}^{K-1}h^a_{\alpha'\beta'}[n',l']\,e^{-j2\pi\frac{k'l'}{K}}\right)\right\} \\ &=\frac{1}{K}\sum_{l=0}^{K-1}\sum_{l'=0}^{K-1}E\left\{h^a_{\alpha\beta}[n,l]\left(h^a_{\alpha'\beta'}[n',l']\right)^*\right\}e^{j2\pi\frac{k'l'-kl}{K}} \\ &=\frac{1}{K}\sum_{l=0}^{K-1}r_{h^a_{\alpha\beta,l}}[\Delta n]\,e^{j2\pi l\frac{-\Delta k}{K}}\,\delta[\Delta\alpha]\,\delta[\Delta\beta], \end{aligned} \tag{16}$$

$$\begin{aligned} &r_h[\Delta n,\Delta u,\Delta v,\Delta l] \\ &=E\left\{h_{uv}[n,l]\left(h_{u'v'}[n',l']\right)^*\right\} \\ &=E\left\{\frac{1}{\sqrt{N_r}}\sum_{\alpha=0}^{N_r-1}\left(\frac{1}{\sqrt{N_t}}\sum_{\beta=0}^{N_t-1}h^a_{\alpha\beta}[n,l]\,e^{-j2\pi\frac{v\beta}{N_t}}\right)e^{-j2\pi\frac{u\alpha}{N_r}}\right. \\ &\qquad\times\left(\frac{1}{\sqrt{N_r}}\sum_{\alpha'=0}^{N_r-1}\left(\frac{1}{\sqrt{N_t}}\sum_{\beta'=0}^{N_t-1}h^a_{\alpha'\beta'}[n',l']\,e^{-j2\pi\frac{v'\beta'}{N_t}}\right)\right. \\ &\qquad\left.\left.\times e^{-j2\pi\frac{u'\alpha'}{N_r}}\right)^*\right\} \\ &=\frac{1}{N_tN_r}\sum_{\alpha=0}^{N_r-1}\sum_{\beta=0}^{N_t-1}r_{h^a_{\alpha\beta,l}}[\Delta n]\,e^{j2\pi\beta\frac{-\Delta v}{N_t}}e^{j2\pi\alpha\frac{-\Delta u}{N_r}}\delta[\Delta l], \end{aligned} \tag{17}$$

$$\begin{aligned} &r_H[\Delta n,\Delta u,\Delta v,\Delta k] \\ &=E\left\{H_{uv}[n,k]\left(H_{u'v'}[n',k']\right)^*\right\} \\ &=\frac{1}{N_tN_rK}\sum_{\alpha=0}^{N_r-1}\sum_{\beta=0}^{N_t-1}\sum_{l=0}^{K-1}r_{h^a_{\alpha\beta,l}}[\Delta n]\,e^{j2\pi l\frac{-\Delta k}{K}}e^{j2\pi\beta\frac{-\Delta v}{N_t}} \\ &\quad\times e^{j2\pi\alpha\frac{-\Delta u}{N_r}}, \end{aligned} \tag{18}$$

where $\Delta k = k - k'$, $\Delta u = u - u'$, and $\Delta v = v - v'$.

IV. mmWave MIMO-OFDM CHANNEL PREDICTION TECHNIQUES

To predict the radio channel in each representation, we should first obtain the channel estimates in each representation. In mmWave MIMO-OFDM systems, channel estimation is usually conducted in the AR-FD as (5), and the channel estimations in other domains can be transformed from the AR-FD channel estimates according to the relationships in Fig 2. As the coherent signal detection and adaptive transmission are performed in the AR-FD, the prediction results in other domain representations should be transformed back into AR-FD. In the following, we introduce the channel prediction technique in each domain.

A. AR-FD CHANNEL PREDICTION

For $k = 0, 1, \cdots, K-1$, the MMSE channel prediction can be performed on each entry of the estimated AR-FD channel

$\tilde{\boldsymbol{H}}[n,k]$ as

$$\hat{H}_{uv}[n+M,k]=\sum_{p=0}^{P-1}d_{H_{uv,k}}(p)\tilde{H}_{uv}[n-pM,k], \quad (19)$$

where P is the prediction order, M is the sample (pilot) interval, and $d_{H_{uv,k}}(p)$, for $p=0,1,\cdots,P-1$ are the optimal prediction coefficients in the MMSE mean for the kth subcarrier from the vth transmitter to the uth receiver. The prediction coefficient in the vector form $\boldsymbol{d}_{H_{uv,k}}=\left[d_{H_{uv,k}}(0),d_{H_{uv,k}}(1),\cdots,d_{H_{uv,k}}(P-1)\right]^T$ can be computed as

$$\boldsymbol{d}_{H_{uv,k}}=\left(\boldsymbol{R}_{H_{uv,k}}+\sigma^2\boldsymbol{I}\right)^{-1}\boldsymbol{r}_{H_{uv,k}}, \quad (20)$$

where

$$\boldsymbol{r}_{H_{uv,k}}=\left[r_{H_{uv,k}}[M],r_{H_{uv,k}}[2M],\cdots,r_{H_{uv,k}}[PM]\right]^T, \quad (21)$$

and $\boldsymbol{R}_{H_{uv,k}}$ is given in (22), as shown at the top of the next page. The elements of $\boldsymbol{R}_{H_{uv,k}}$ and $\boldsymbol{r}_{H_{uv,k}}$ can be given as

$$r_{H_{uv,k}}[nM]=r_H[nM,0,0,0], \quad n=0,1,\cdots,P.$$

The MSE of the predicted AR-FD channel can be given as

$$MSE_{AR-FD}=\frac{1}{N_rN_tK}\sum_{u=0}^{N_r-1}\sum_{v=0}^{N_t-1}\sum_{k=0}^{K-1}\left[r_{H_{uv,k}}[0]-\boldsymbol{r}_{H_{uv,k}}^H\boldsymbol{d}_{H_{uv,k}}\right]. \quad (23)$$

B. AG-FD CHANNEL PREDICTION

Due to the use of MIMO technique, the AR-FD estimates of MIMO-OFDM channel can be transformed into the AG-FD estimates ($\tilde{\boldsymbol{H}}^a[n,k]$) using the relationships in Fig 2. The MMSE prediction for AG-FD channel can be performed on each entry of $\tilde{\boldsymbol{H}}^a[n,k]$ as

$$\hat{H}^a_{\alpha\beta}[n+M,k]=\sum_{p=0}^{P-1}d_{H^a_{\alpha\beta,k}}(p)\tilde{H}^a_{\alpha\beta}[n-pM,k], \quad (24)$$

where $d_{H^a_{\alpha\beta,k}}(p)$, for $p=0,1,\cdots,P-1$ are the optimal prediction coefficients in the MMSE mean, which can be computed in a manner similar to (20). Then, to implement the adaptation in AR-FD, the AG-FD channel prediction will be transformed back into AR-FD according to the relationships in Fig 2. The MSE of the channel predictions should be computed in the AR-FD, and we have

$$\begin{aligned}MSE_{AG-FD}&=\frac{1}{K}\sum_{k=0}^{K-1}\left\|\boldsymbol{H}[n+M,k]-\boldsymbol{U}_r\hat{\boldsymbol{H}}^a[n+M,k]\boldsymbol{U}_t^H\right\|^2\\&=\frac{1}{K}\sum_{k=0}^{K-1}\left\|\boldsymbol{U}_r\left(\boldsymbol{H}^a[n+M,k]-\hat{\boldsymbol{H}}^a[n+M,k]\right)\boldsymbol{U}_t^H\right\|^2\\&=\frac{1}{K}\sum_{k=0}^{K-1}\left\|\boldsymbol{H}^a[n+M,k]-\hat{\boldsymbol{H}}^a[n+M,k]\right\|^2. \quad (25)\end{aligned}$$

From (25), we know that when the channel prediction is conducted in the AG-FD, the MSE can be directly computed in the AG-FD without needing to be transformed back to the AR-FD. The same rule can also be applied to the other domain techniques. Then, the MSE of the AG-FD channel predicts can be given as

$$MSE_{AG-FD}=\frac{1}{N_rN_tK}\sum_{\alpha=0}^{N_r-1}\sum_{\beta=0}^{N_t-1}\sum_{k=0}^{K-1}\left[r_{H^a_{\alpha\beta,k}}[0]-\boldsymbol{r}_{H^a_{\alpha\beta,k}}^H\boldsymbol{d}_{H^a_{\alpha\beta,k}}\right], \quad (26)$$

where $\boldsymbol{d}_{H^a_{\alpha\beta,k}}$ is the channel prediction vector, $\boldsymbol{r}_{H^a_{\alpha\beta,k}}$ is the AG-FD channel correlation vector, and for $n=0,1,\cdots,P$, $r_{H^a_{\alpha\beta,k}}[nM]=r_{H^a}[nM,0,0,0]$.

C. AR-TD CHANNEL PREDICTION

Using the relationships in Fig 2, the AR-TD channel estimates from the vth transmitter to the uth receiver at delay l can be obtained as $\tilde{h}_{uv}[n,l]$. Then, the MMSE channel prediction can be performed in the AR-TD as

$$\hat{h}_{uv}[n+M,l]=\sum_{p=0}^{P-1}d_{h_{uv,l}}(p)\tilde{h}_{uv}[n-pM,l], \quad (27)$$

where $d_{h_{uv,l}}(p)$, for $p=0,1,\cdots,P-1$ are the prediction coefficients obtained by minimizing the MSE of the predicted AR-TD channel. We can directly give out the MSE of AR-TD technique as

$$MSE_{AR-TD}=\frac{1}{N_rN_tK}\sum_{u=0}^{N_r-1}\sum_{v=0}^{N_t-1}\sum_{l=0}^{K-1}\left[r_{h_{uv,l}}[0]-\boldsymbol{r}_{h_{uv,l}}^H\boldsymbol{d}_{h_{uv,l}}\right], \quad (28)$$

where $\boldsymbol{d}_{h_{uv,l}}$ is the channel prediction vector, $\boldsymbol{r}_{h_{uv,l}}$ is the AR-TD channel correlation vector, and for $n=0,1,\cdots,P$, $r_{h_{uv,l}}[nM]=r_h[nM,0,0,0]$.

D. AG-TD CHANNEL PREDICTION

To obtain the AG-TD channel estimates ($\tilde{\boldsymbol{h}}^a[n,l]$) from the AR-FD estimates, two transformations should be conducted as shown in Fig 2: the first transformation is from the FD to the TD, and the second one is from the ARD to the AGD. Then, the MMSE channel prediction can be performed in the AG-TD as

$$\hat{h}^a_{\alpha\beta}[n+M,l]=\sum_{p=0}^{P-1}d_{h^a_{\alpha\beta,l}}(p)\tilde{h}^a_{\alpha\beta}[n-pM,l], \quad (29)$$

where $d_{h^a_{\alpha\beta,l}}(p)$, for $p=0,1,\cdots,P-1$ are the prediction coefficients. The MSE of the predicted AG-TD channel is

$$MSE_{AG-TD}=\frac{1}{N_rN_tK}\sum_{\alpha=0}^{N_r-1}\sum_{\beta=0}^{N_t-1}\sum_{l=0}^{K-1}\left[r_{h^a_{\alpha\beta,l}}[0]-\boldsymbol{r}_{h^a_{\alpha\beta,l}}^H\boldsymbol{d}_{h^a_{\alpha\beta,l}}\right], \quad (30)$$

where $\boldsymbol{d}_{h^a_{\alpha\beta,l}}$ is the channel prediction vector, $\boldsymbol{r}_{h^a_{\alpha\beta,l}}$ is the AG-TD channel correlation vector, and for $n=0,1,\cdots,P$, $r_{h^a_{\alpha\beta,l}}[nM]=r_{h^a}[nM,0,0,0]$.

$$\boldsymbol{R}_{H_{uv,k}} = \begin{bmatrix} r_{H_{uv,k}}[0] & r^*_{H_{uv,k}}[M] & \cdots & r^*_{H_{uv,k}}[(P-1)M] \\ r_{H_{uv,k}}[M] & r_{H_{uv,k}}[0] & \cdots & r^*_{H_{uv,k}}[(P-2)M] \\ \vdots & \vdots & \ddots & \vdots \\ r_{H_{uv,k}}[(P-1)M] & r_{H_{uv,k}}[(P-2)M] & \cdots & r_{H_{uv,k}}[0] \end{bmatrix}. \tag{22}$$

V. PERFORMANCE COMPARISON

In this section, we evaluate the MSE performance and computational complexity of different prediction techniques. For the MSE performance comparison, we express MSE results of all the predictors in a uniform way by converting all the other domain MSE results into the AG-TD. For the computational complexity comparison, we focus on the computational complexity for both the MMSE channel prediction and the transformations among different domains.

A. MSE COMPARISON

The MSE of the AG-TD channel prediction is given in (30), and we rewrite it as follows for clarity

$$MSE_{AG-TD} = \frac{1}{N_r N_t K}\sum_{\alpha=0}^{N_r-1}\sum_{\beta=0}^{N_t-1}\sum_{l=0}^{K-1}\left[r_{h^a_{\alpha\beta,l}}[0] - \boldsymbol{r}^H_{h^a_{\alpha\beta,l}}\boldsymbol{d}_{h^a_{\alpha\beta,l}}\right]. \tag{31}$$

In the following, we convert the prediction MSE results of the other domains into the AG-TD.

Based on the channel statistic relationship in equation (16), the MSE of AG-FD prediction (26) can be derived by

$$\begin{aligned} MSE_{AG-FD} &= \frac{1}{N_r N_t K}\sum_{\alpha=0}^{N_r-1}\sum_{\beta=0}^{N_t-1}\sum_{k=0}^{K-1}\left[r_{H^a_{\alpha\beta,k}}[0] - \boldsymbol{r}^H_{H^a_{\alpha\beta,k}}\boldsymbol{d}_{H^a_{\alpha\beta,k}}\right] \\ &= \frac{1}{N_r N_t K}\sum_{\alpha=0}^{N_r-1}\sum_{\beta=0}^{N_t-1}\sum_{k=0}^{K-1}\left[\frac{1}{K}\sum_{l=0}^{K-1} r_{h^a_{\alpha\beta,l}}[0] - \left(\frac{1}{K}\sum_{l=0}^{K-1}\boldsymbol{r}_{h^a_{\alpha\beta,l}}\right)^H \boldsymbol{d}_{H^a_{\alpha\beta,k}}\right] \\ &= \frac{1}{N_r N_t K}\sum_{\alpha=0}^{N_r-1}\sum_{\beta=0}^{N_t-1}\sum_{l=0}^{K-1}\left[r_{h^a_{\alpha\beta,l}}[0] - \boldsymbol{r}^H_{h^a_{\alpha\beta,l}}\left(\boldsymbol{d}_{H^a_{\alpha\beta,\bar{k}}}\right)\right], \end{aligned} \tag{32}$$

where

$$\boldsymbol{d}_{H^a_{\alpha\beta,\bar{k}}} = \frac{1}{K}\sum_{l=0}^{K-1}\left(\boldsymbol{d}_{H^a_{\alpha\beta,k}}\right).$$

The MSE of AG-TD channel prediction method is given in (31), while the MSE of AR-TD channel prediction method is given in (32). Comparing (31) with the last line of (32), we can find that the only difference between the two equations is the prediction vector. The prediction vector $\boldsymbol{d}_{h^a_{\alpha\beta,l}}$ in (31) is the optimal prediction coefficient vector in the MMSE mean for the corresponding AG-TD element, while the prediction vector $\boldsymbol{d}_{H^a_{\alpha\beta,\bar{k}}}$ in (32) is not. It means that the prediction vector $\boldsymbol{d}_{h^a_{\alpha\beta,l}}$ can predict the AG-TD channel more accurate than other prediction vectors [45]. Therefore, we have

$$r_{h^a_{\alpha\beta,l}}[0] - \boldsymbol{r}^H_{h^a_{\alpha\beta,l}}\boldsymbol{d}_{h^a_{\alpha\beta,l}} \le r_{h^a_{\alpha\beta,l}}[0] - \boldsymbol{r}^H_{h^a_{\alpha\beta,l}}\boldsymbol{d}_{H^a_{\alpha\beta,\bar{k}}}. \tag{33}$$

Hence, we have

$$MSE_{AG-TD} \le MSE_{AG-FD}. \tag{34}$$

Based on the channel statistic relationship in equation (17), the MSE of AR-TD prediction (28) can be deduced as

$$\begin{aligned} MSE_{AR-TD} &= \frac{1}{N_r N_t K}\sum_{u=0}^{N_r-1}\sum_{v=0}^{N_t-1}\sum_{l=0}^{K-1}\left[r_{h_{uv,l}}[0] - \boldsymbol{r}^H_{h_{uv,l}}\boldsymbol{d}_{h_{uv,l}}\right] \\ &= \frac{1}{N_r N_t K}\sum_{u=0}^{N_r-1}\sum_{v=0}^{N_t-1}\sum_{l=0}^{K-1}\left[\frac{1}{N_r N_t}\sum_{\alpha=0}^{N_r-1}\sum_{\beta=0}^{N_t-1} r_{h^a_{\alpha\beta,l}}[0] - \frac{1}{N_r N_t}\left(\sum_{\alpha=0}^{N_r-1}\sum_{\beta=0}^{N_t-1}\boldsymbol{r}_{h^a_{\alpha\beta,l}}\right)^H \boldsymbol{d}_{h_{uv,l}}\right] \\ &= \frac{1}{N_r N_t K}\sum_{l=0}^{K-1}\sum_{\alpha=0}^{N_r-1}\sum_{\beta=0}^{N_t-1}\left[r_{h^a_{\alpha\beta,l}}[0] - \boldsymbol{r}^H_{h^a_{\alpha\beta,l}}\boldsymbol{d}_{h_{\overline{uv},l}}\right], \end{aligned} \tag{35}$$

where

$$\boldsymbol{d}_{h_{\overline{uv},l}} = \frac{1}{N_r N_t}\sum_{u=0}^{N_r-1}\sum_{v=0}^{N_t-1}\boldsymbol{d}_{h_{uv,l}}.$$

For the similar reason as the AG-FD case, we have

$$MSE_{AG-TD} \le MSE_{AR-TD}. \tag{36}$$

For the MSE of the AR-FD channel prediction (23), we have

$$\begin{aligned} MSE_{AR-FD} &= \frac{1}{N_r N_t K}\sum_{u=0}^{N_r-1}\sum_{v=0}^{N_t-1}\sum_{k=0}^{K-1}\left[r_{H_{uv,k}}[0] - \boldsymbol{r}^H_{H_{uv,k}}\boldsymbol{d}_{H_{uv,k}}\right] \\ &= \frac{1}{N_r N_t K}\sum_{u=0}^{N_r-1}\sum_{v=0}^{N_t-1}\sum_{k=0}^{K-1}\left[\frac{1}{K}\sum_{l=0}^{K-1} r_{h_{uv,l}}[0] - \frac{1}{K}\left(\sum_{l=0}^{K-1}\boldsymbol{r}_{h_{uv,l}}\right)^H \boldsymbol{d}_{H_{uv,k}}\right] \end{aligned}$$

TABLE 1. Computational complexity.

Method	Transformation	Prediction
Array-frequency	0	$O\left(N_r N_t K p^2\right)$
Array-time	$O\left(N_r N_t K \log_2 K\right)$	$O\left(N_r N_t K p^2\right)$
Angle-frequency	$O\left(N_r N_t K \left(2N_r + 2N_t\right)\right)$	$O\left(N_r N_t K p^2\right)$
Angle-time	$O\left(N_r N_t K \left(2N_r + 2N_t + \log_2 K\right)\right)$	$O\left(N_r N_t K p^2\right)$

$$= \frac{1}{N_r N_t K} \sum_{u=0}^{N_r-1} \sum_{v=0}^{N_t-1} \sum_{l=0}^{K-1} \left[r_{h_{uv,l}}[0] - \boldsymbol{r}_{h_{uv,l}}^H \boldsymbol{d}_{H_{uv,\bar{k}}} \right], \quad (37)$$

where

$$\boldsymbol{d}_{H_{uv,\bar{k}}} = \frac{1}{K} \sum_{l=0}^{K-1} \boldsymbol{d}_{H_{uv,k}}.$$

In (37), the MSE of AR-FD channel prediction is expressed in the AR-TD, and the only difference with MSE of AR-TD predictor (in the second line of (35)) is the prediction coefficient vector. As $\boldsymbol{d}_{h_{uv,l}}$ in (35) is the optimal prediction coefficient vector in the MMSE mean for the corresponding AR-TD element, we can obtain

$$MSE_{AR-TD} \leq MSE_{AR-FD}. \quad (38)$$

Based on (36) and (38), we have

$$MSE_{AG-TD} \leq MSE_{AR-TD} \leq MSE_{AR-FD}. \quad (39)$$

In (37), the MSE is first transformed from the AR-FD into the AR-TD, and then into the AG-TD. We can also operate the transformation from the AR-FD first into the AG-FD, and then into the AG-TD. In this way, we have

$$MSE_{AG-TD} \leq MSE_{AG-FD} \leq MSE_{AR-FD}. \quad (40)$$

From equations (34), (36), (39), and (40), we know that the AG-TD channel prediction technique achieves a better MSE performance compared with the other three domain methods.

B. COMPUTATIONAL COMPLEXITY

We detail the computational complexity for both the MMSE channel prediction and the transformations among different domains. The MMSE channel prediction technique can compute optimal predictor coefficients using the Levinson recursion, and its computational complexity is $O\left(p^2\right)$. Meanwhile, two types of transformations are employed in the proposed prediction techniques: the first type is the transformation between the ARD and the AGD, which requires a computational complexity of $2N_r + 2N_t$ for each channel coefficient; the second one is the transformation between the FD and the TD, which gives a computational complexity of $\log_2 K$ (the DFT/IDFT can be conducted using FFT/IFFT) for each channel coefficient. The computational complexity of the predictors studied in this paper is summarized in Table 1. It can be seen that the transformation complexity does not affect the total computational order.

C. DISCUSSION

We have analyzed the MSE performance and computational complexity of the channel prediction techniques in the four domains, i.e., the AG-TD, AG-FD, AR-TD, and AR-FD. In the following, we will provide an insight into the above analytical results. As the prediction parameters used in any of the four domains are the same, the accuracy of the prediction in each domain should be decided by the channel structure of the corresponding domain. In Section III, we have described the channel representations of the four domains in detail, from which we can gain insights into the channel structure of each domain.

There is a clear analogy between an OFDM system and a MIMO system. In both systems, a transformation can be applied to convert the radio channel from a complicated representation into a simple representation. In OFDM systems, an IDFT can be employed to transform the FD channel subcarriers into the TD channel taps, i.e., each OFDM subcarrier in the FD is a combination of all the channel taps in the TD. As each tap arises due to contributions from different multipath scatterers, the physical paths in each tap are fewer than those in the subcarrier which is composed of all the channel taps. Therefore, the TD channel tap is more predictable than the FD channel subcarrier. In MIMO systems, the ARD channel representation can be transformed into AGD representation via a two-dimensional Fourier transformation, and thus each ARD channel element is a combination of all the elements in the AGD. As different physical paths contribute to different AGD elements, the physical paths in each AGD element are fewer than those in the ARD element. Therefore, the AGD channel element is more predictable than the ARD channel element. Based on the above discussions, it is obvious that the AR-TD channel should be the most predictable among the four channel representations.

It should be noted that there are some other prediction methods except for MMSE prediction, such as least mean square (LMS), recursive least square (RLS), root multiple signal classification (Root-MUSIC) and estimation of signal parameters via rotational invariance techniques (ESPRIT) [21], [46], [47]. The performance of those channel prediction methods (MMSE, LMS, RLS, Root-MUSIC and ESPRIT) may be different. However, the comparison results among the four domain representations of each prediction method are similar. In this paper, our main focus is to investigate the effects of channel representations (AG-TD, AG-FD, AR-TD, AR-FD) on channel prediction method. So we only take MMSE prediction method as an example.

VI. ENHANCED ANGLE-TIME DOMAIN CHANNEL PREDICTION

To further improve the AG-TD channel prediction method, we exploit the mmWave MIMO-OFDM channel sparsity in both the time and the angle domains. The enhanced algorithm can be divided into two stages: the first stage is to identify the significant channel tap positions, and the second one is

to identify the significant AGD coefficients of the significant channel taps. In this section, we also briefly discuss the prediction performance improvement of the enhanced AG-TD channel predictor over the normal one proposed in Section IV.

We first transform the AR-FD channel estimates into the AR-TD, and identify the nonzero channel tap positions. After the transformation, we can obtain the AR-TD channel estimates $\tilde{\boldsymbol{h}}[n,l]$. As the channel's maximum delay usually does not exceed the CP length of OFDM system L_{cp}, for $l = L_{cp}, L_{cp}+1, \cdots, K-1$, we have

$$\tilde{\boldsymbol{h}}[n,l] = \boldsymbol{z}[n,l], \tag{41}$$

where $\boldsymbol{z}[n,l]$ is the noise matrix in the AR-TD, and its (u,v) th entry is $z_{uv}[n,l]$. The radio channel is often sparse in the TD, so for $l = 0, 1, \cdots, L_{cp}-1$, $\tilde{\boldsymbol{h}}[n,l]$ can be written as

$$\tilde{\boldsymbol{h}}[n,l] = \begin{cases} \boldsymbol{h}[n,l] + \boldsymbol{z}[n,l], & \text{significant tap} \\ \boldsymbol{z}[n,l], & \text{zero-valued tap.} \end{cases} \tag{42}$$

Then, we give the nonzero channel taps identification algorithm as

$$\begin{aligned} &\text{for } l = 0, 1, \cdots, L_{cp}-1 \\ &\tilde{\boldsymbol{h}}[n,l] = \begin{cases} \tilde{\boldsymbol{h}}[n,l], & \text{if } \sigma^2_{h_l} - \sigma_t^2 \geq \sigma_t^2 \\ 0, & \text{if } \sigma^2_{h_l} - \sigma_t^2 < \sigma_t^2 \end{cases} \\ &\text{for } l = L_{cp}, L_{cp}+1, \cdots, K-1 \\ &\text{set } \tilde{\boldsymbol{h}}[n,l] = 0, \end{aligned}$$

where $\sigma^2_{h_l} = E\left\{\left\|\tilde{\boldsymbol{h}}[n,l]\right\|^2\right\}$ is the average power of the lth AR-TD channel tap computed from the past channel estimates, and σ_t^2 is the noise power of each tap estimated by

$$\sigma_t^2 = \frac{1}{K - L_{cp}} \sum_{l=L_{cp}}^{K-1} \sigma^2_{h_l}.$$

Secondly, for each significant channel tap, as some AGD bins contain no physical sinusoid due to limited scattering, the corresponding channel coefficients approach zeros. We transform the identified AR-TD channel $\tilde{\boldsymbol{h}}[n,l]$ into the AG-TD channel $\tilde{\boldsymbol{h}}^a[n,l]$ using the relationships in Fig 2. If the lth channel tap is significant, we can further identify the significant AGD coefficients of this channel tap as

$$\tilde{h}^a_{\alpha\beta}[n,l] = \begin{cases} \tilde{h}^a_{\alpha\beta}[n,l], & \text{if } \sigma^2_{h^a_{\alpha\beta,l}} - \sigma_a^2 \geq \sigma_a^2 \\ 0, & \text{if } \sigma^2_{h^a_{\alpha\beta,l}} - \sigma_a^2 < \sigma_a^2, \end{cases} \tag{43}$$

where

$$\sigma^2_{h^a_{\alpha\beta,l}} = E\left\{\left|\tilde{h}^a_{\alpha\beta}[n,l]\right|^2\right\}$$

is the average power of the channel from the βth transmit angle to the αth receive angle in the lth channel tap, and σ_a^2 is the noise power of each AG-TD bin estimated by

$$\sigma_a^2 = \frac{1}{(K - L_{cp})N_r N_t} \sum_{l=L_{cp}}^{K-1} \sum_{\alpha=0}^{N_r-1} \sum_{\beta=0}^{N_t-1} \sigma^2_{h^a_{\alpha\beta,l}}.$$

Finally, the channel prediction can be performed on each significant element in the AG-TD, and the details are similar to the AG-TD channel prediction technique.

The enhanced AG-TD channel prediction technique only performs MMSE predictors on the significant angle elements of the significant channel taps, for which it can eliminate the noise perturbation and make the prediction more accurate. If the wireless channel contains L_{st} significant channel taps, and the lth ($l = 0, 1, \cdots, L_{st}-1$) significant channel tap contains $L_r(l)$ significant receive AGD elements and $L_t(l)$ significant transmit AGD elements, then the enhanced AG-TD channel prediction technique can eliminate the noise at a ratio

$$\eta_{\text{eliminate}} = \frac{KN_rN_t - \sum_{l=0}^{L_{st}-1} L_r(l) L_t(l)}{KN_rN_t}. \tag{44}$$

Moreover, the enhanced AG-TD technique only performs prediction on the significant channel elements, and thus its computational complexity for prediction is

$$O\left(\sum_{l=0}^{L_{st}-1} L_r(l) L_t(l) p^2\right),$$

which reduces the prediction complexity a lot.

VII. SIMULATION RESULTS

In this section, we show the performance of different channel prediction techniques in terms of the normalized mean-square-error (NMSE), defined as

$$\text{NMSE} = \frac{E\left[\left\|\boldsymbol{H}[n] - \hat{\boldsymbol{H}}[n]\right\|^2\right]}{E\left[\|\boldsymbol{H}[n]\|^2\right]}, \tag{45}$$

where

$$\begin{aligned} \boldsymbol{H}[n] &= [\boldsymbol{H}[n,0], \boldsymbol{H}[n,1], \cdots, \boldsymbol{H}[n,K-1]]^T \\ \hat{\boldsymbol{H}}[n] &= \left[\hat{\boldsymbol{H}}[n,0], \hat{\boldsymbol{H}}[n,1], \cdots, \hat{\boldsymbol{H}}[n,K-1]\right]^T. \end{aligned} \tag{46}$$

are the real and the predicted AR-FD channel matrices, respectively. Before presenting the simulation results, we first describe the parameters of the simulated MIMO-OFDM system.

A. PARAMETERS OF mmWave MIMO-OFDM SYSTEM

In this paper, we use the standardized 3GPP channel models [48], which support comparisons across frequency bands over the range 0.5-100 GHz, to test our prediction algorithms. In wireless communications, the mmWave ground/near-ground MIMO channel is mainly composed of non-line-of-sight (NLOS) component [49], while the

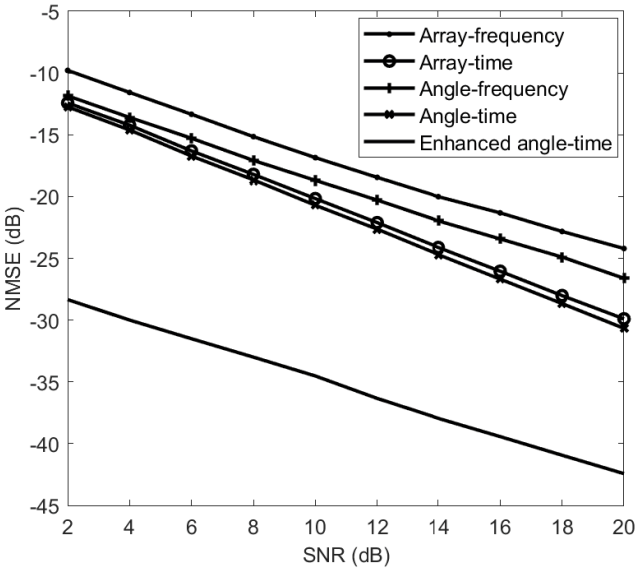

FIGURE 3. NMSE performance versus SNR for NLOS condition. $K = 512$, $N_r = N_t = 4$.

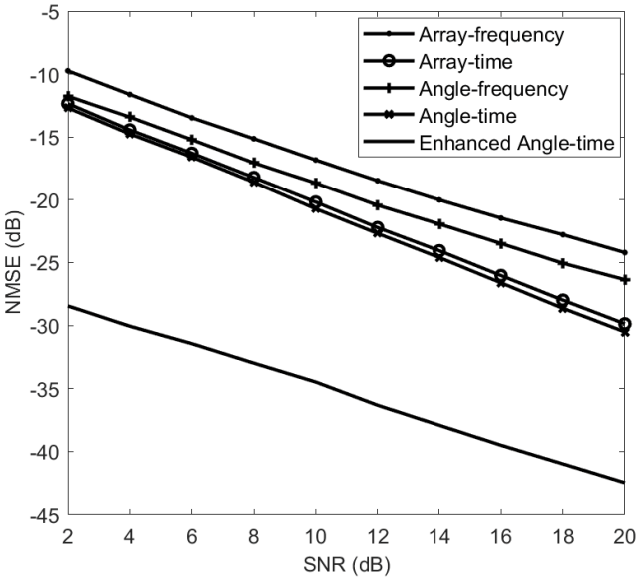

FIGURE 4. NMSE performance versus SNR for LOS condition. $K = 512$, $N_r = N_t = 4$.

mmWave airborne MIMO channel is composed of LOS component and NLOS component [50]. Therefore, we consider both the LOS and NLOS conditions for the comparisons. In this paper, we construct the mmWave CIR by using the clustered delay line (CDL) channel model with delay profile CDL-B and CDL-D from TR 38.901 [48]. The CDL-B is constructed to represent channel profile for NLOS while CDL-D is constructed for LOS. It should be noted that the CDL-B and CDL-D of 3GPP TR 38.901 are double directional 3D channel models with both azimuth and elevation angles, and only azimuth angle is considered in this paper. The maximum Doppler shift is set as $f_{\max} = 1.67$ kHz (an example of this is when the carrier frequency is 50 GHz and the velocity of MS is about 10 m/s). The data sampling rate is set as 100 MHz, while the sampling rate used for channel estimation is set as $f_s = 8f_{\max}$, which is much lower than the data rate and higher than double of the maximum Doppler shift. In this simulation, 200 channel samples are generated. The first 100 samples are used for computing the MMSE prediction coefficients, while the second 100 samples for performance evaluation. The CP length L_{cp} is set as $1/4K$ (K is the subcarrier number of OFDM), which is larger than the maximum channel delay. We set the normalized separation between antennas as $\Delta_r = \Delta_t = 0.5$.

B. SIMULATION RESULTS

To make a fair prediction accuracy comparison among the proposed techniques, we set the order $p = 10$ for all the predictors, and normalize the channel power to 1. Fig. 3 shows the NMSE performance versus SNR for NLOS condition. It can be seen that the AG-TD technique is more accurate than the other three domain techniques, and the enhanced AG-TD method can further improve the accuracy. Fig. 4 shows the NMSE performance versus SNR for LOS condition, and it has similar comparison results to the NLOS case. The prediction performance presented in the simulations reveals that the analysis in Section V is effective for both conditions.

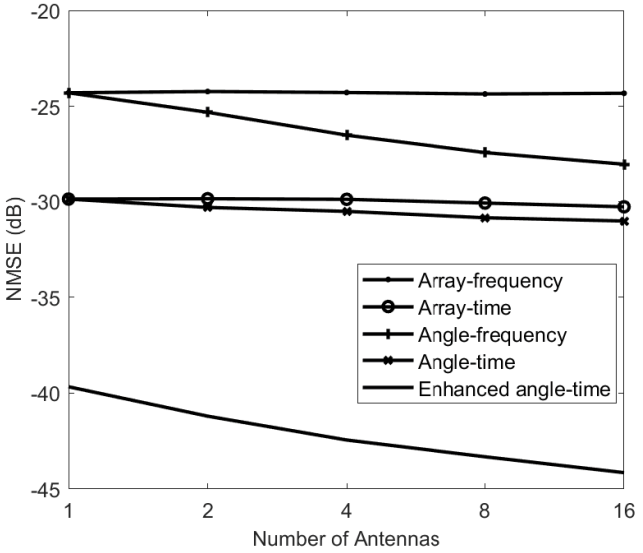

FIGURE 5. NMSE performance versus antenna number ($N_r = N_t$) for NLOS condition. $SNR = 20dB$, $K = 512$.

Fig. 5 and Fig. 6 show the NMSE performance versus antenna number for NLOS and LOS conditions, respectively. It can be seen that, for both cases, the antenna number affects the prediction accuracy of AGD prediction techniques. As the antenna number increases, the angular resolution will be higher, which causes each angular bin to contain contributions from a lower number of paths. Therefore, the AGD prediction techniques will be more accurate with larger antenna

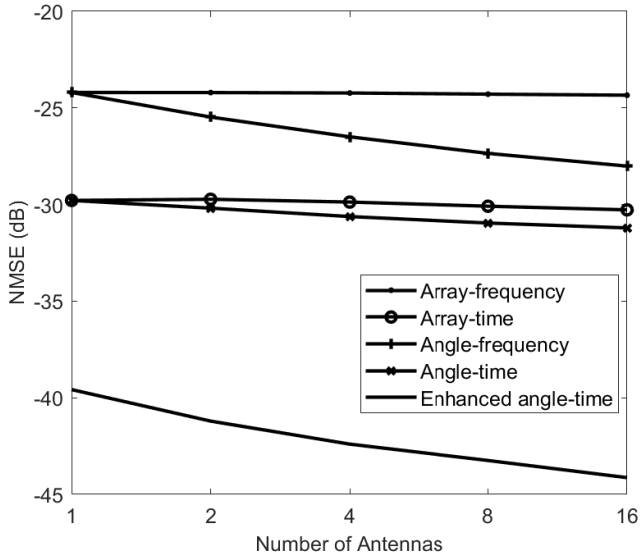

FIGURE 6. NMSE performance versus antenna number ($N_r = N_t$) for LOS condition. $SNR = 20dB$, $K = 512$.

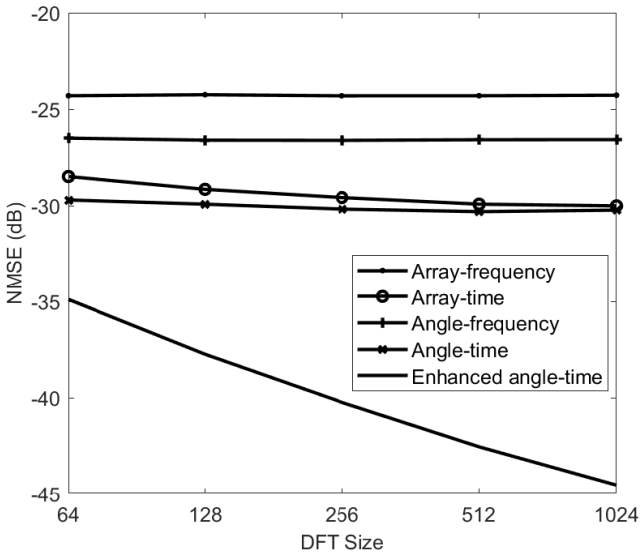

FIGURE 7. NMSE performance versus DFT size (K) for NLOS condition. $SNR = 20dB$, $N_r = N_t = 4$.

number. It can also be observed that the ARD techniques almost keep constant with the increase of antenna number, because the ARD techniques take no benefit from the increase of antenna number. In particular, as the antenna number increases, the performance gain of the enhanced AG-TD method over non-enhanced predictor increases, because more angle domain noise perturbation is eliminated.

Fig. 7 and Fig. 8 show the NMSE performance versus FFT size for NLOS and LOS conditions, respectively. It can be seen that, for both cases, the FFT size affects the prediction accuracy of the TD prediction techniques. As the FFT size increases, the frequency band is wider, and thus the temporal resolution in the channel impulse response becomes higher. In this case, the channel taps with different delays

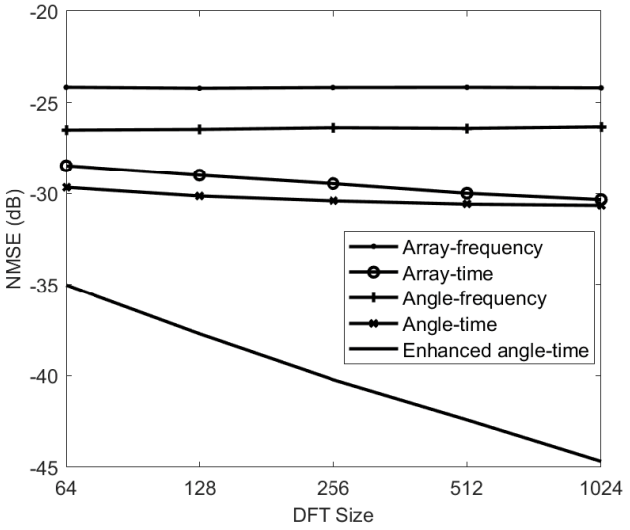

FIGURE 8. NMSE performance versus DFT size (K) for LOS condition. $SNR = 20dB$, $N_r = N_t = 4$.

can be resolved more accurately, and thus the TD prediction techniques could be more accurate with a larger FFT size. It can also be observed that the FD techniques almost keep constant with the increase of FFT size, because the FD techniques take no benefit from the increase of FFT size. In particular, as the FFT size increases, the performance gain of the enhanced AG-TD method over non-enhanced method increases, because more TD noise perturbation is eliminated.

VIII. CONCLUSION

In mmWave MIMO-OFDM communications, motivated by the fact that the CSI based on channel estimation may be outdated for signal detection and adaptive transmission, the authors investigate channel prediction to obtain prior CSI in doubly-selective Fading Channels. We first represent the channel in the AR-FD, the AR-TD, the AG-FD, and the AG-TD, and investigate their relationships and statistics. Then, we derive the channel prediction techniques in the four domains, and study how the channel representations affect the prediction techniques. We analyze the performance of the proposed predictors, and it is presented that the prediction technique in the AG-TD can provide a higher accuracy than the prediction techniques in the other three domains. We also propose an enhanced AG-TD prediction method which improve the prediction accuracy by eliminating the noise perturbation in both the angle and the time domains. Finally, simulations are conducted to validate the correctness of our analysis. Furthermore, the results also show that the accuracy using the AGD prediction techniques is improved as the increase of the antenna number, while the accuracy using the TD techniques is improved as the increase of the FFT size.

REFERENCES

[1] G. L. Stüber, J. R. Barry, S. W. McLaughlin, Y. Li, M. A. Ingram, and T. G. Pratt, "Broadband MIMO-OFDM wireless communications," *Proc. IEEE*, vol. 92, no. 2, pp. 271–294, Feb. 2004.

[2] J. Mietzner, R. Schober, L. Lampe, W. H. Gerstacker, and P. A. Hoeher, "Multiple-antenna techniques for wireless communications—A comprehensive literature survey," *IEEE Commun. Surveys Tuts.*, vol. 11, no. 2, pp. 87–105, 2nd Quart., 2009.
[3] J.-C. Lin,"Channel estimation for wireless OFDM communications," in *Communications and Networking*, InTech, 2010, ch. 2.
[4] T. S. Rappaport *et al.*, *Millimeter Wave Wireless Communications*. Upper Saddle River, NJ, USA: Prentice-Hall, 2014.
[5] S. A. Busari, S. Mumtaz, S. Al-Rubaye, and J. Rodriguez, "5G millimeter-wave mobile broadband: Performance and challenges," *IEEE Commun. Mag.*, vol. 56, no. 6, pp. 137–143, Jun. 2018.
[6] L. Yang, Y. Zeng, and R. Zhang, "Channel estimation for millimeter-wave MIMO communications with lens antenna arrays," *IEEE Trans. Veh. Technol.*, vol. 67, no. 4, pp. 3239–3251, Apr. 2018.
[7] L. Huang, Y. Wang, Z. Shi, and R. Wen, "Radio parameter design for OFDM-based millimeter-wave systems," in *Proc. IEEE 27th Annu. Int. Symp. Pers., Indoor, Mobile Radio Commun.*, Valencia, Spain, Sep. 2016, pp. 1–5.
[8] J. He, T. Kim, H. Ghauch, K. Liu, and G. Wang, "Millimeter wave MIMO channel tracking systems," in *Proc. IEEE Globecom Workshops*, Austin, TX, USA, Dec. 2014, pp. 416–421.
[9] R. W. Heath, Jr., N. González-Prelcic, S. Rangan, W. Roh, and A. M. Sayeed, "An overview of signal processing techniques for millimeter wave MIMO systems," *IEEE J. Sel. Topics Signal Process.*, vol. 10, no. 3, pp. 436–453, Apr. 2016.
[10] Z. Xiao, P. Xia, and X.-G. Xia, "Channel estimation and hybrid precoding for millimeter-wave MIMO systems: A low-complexity overall solution," *IEEE Access*, vol. 5, pp. 16100–16110, 2017.
[11] M.-T. Martinez-Ingles, C. Sanchis-Borras, J.-M. Molina-Garcia-Pardo, J.-V. Rodríguez, and L. Juan-Llácer, "Experimental evaluation of an indoor MIMO-OFDM system at 60 GHz based on the IEEE802.15.3c standard," *IEEE Antennas Wireless Propag. Lett.*, vol. 12, pp. 1562–1565, 2013.
[12] Y.-P. Lin, "Hybrid MIMO-OFDM beamforming for wideband mmWave channels without instantaneous feedback," *IEEE Trans. Signal Process.*, vol. 66, no. 19, pp. 5142–5151, Oct. 2018.
[13] F. Sohrabi and W. Yu, "Hybrid analog and digital beamforming for mmWave OFDM large-scale antenna arrays," *IEEE J. Sel. Areas Commun.*, vol. 35, no. 7, pp. 1432–1443, Jul. 2017.
[14] P. Zhou *et al.*, "IEEE 802.11ay-based mmWave WLANs: Design challenges and solutions," *IEEE Commun. Surveys Tuts.*, vol. 20, no. 3, pp. 1654–1681, 3rd Quart., 2018.
[15] M. Mezzavilla *et al.*, "Public safety communications above 6 GHz: Challenges and opportunities," *IEEE Access*, vol. 6, pp. 316–329, 2017.
[16] S. Rangan, T. S. Rappaport, and E. Erkip, "Millimeter-wave cellular wireless networks: Potentials and challenges," *Proc. IEEE*, vol. 102, no. 3, pp. 366–385, Mar. 2014.
[17] Q. Qin, L. Gui, P. Cheng, and B. Gong, "Time-varying channel estimation for millimeter wave multiuser MIMO systems," *IEEE Trans. Veh. Technol.*, vol. 67, no. 10, pp. 9435–9448, Oct. 2018.
[18] W. Peng, M. Zou, and T. Jiang, "Channel prediction in time-varying massive MIMO environments," *IEEE Access*, vol. 5, pp. 23938–23946, 2017.
[19] Y. Li, "Pilot-symbol-aided channel estimation for OFDM in wireless systems," *IEEE Trans. Veh. Technol.*, vol. 49, no. 4, pp. 1207–1215, Jul. 2000.
[20] T. L. Jensen, S. Kant, J. Wehinger, and B. H. Fleury, "Fast link adaptation for MIMO OFDM," *IEEE Trans. Veh. Technol.*, vol. 59, no. 8, pp. 3766–3778, Oct. 2010.
[21] A. Duel-Hallen, "Fading channel prediction for mobile radio adaptive transmission systems," *Proc. IEEE*, vol. 95, no. 12, pp. 2299–2313, Dec. 2007.
[22] A. Duel-Hallen, S. Hu, and H. Hallen, "Long-range prediction of fading signals: Enabling adaptive transmission for mobile radio channels," *IEEE Signal Process. Mag.*, vol. 17, no. 3, pp. 62–75, May 2000.
[23] T. Ekman, "Prediction of mobile radio channels: Modeling and design," Ph.D. dissertation, Dept. Eng. Sci., Uppsala Univ., Uppsala, Sweden, Oct. 2002.
[24] A. Heidari, A. K. Khandani, and D. Mcavoy, "Adaptive modelling and long-range prediction of mobile fading channels," *IET Commun.*, vol. 4, no. 1, pp. 39–50, 2010.
[25] L. Liu, H. Feng, B. Hu, and J. Zhang, "MIMO-OFDM wireless channel prediction by exploiting spatial correlation," in *Proc. IEEE Int. Conf. Wireless Commun. Signal Process.*, Oct. 2012, pp. 1–6.
[26] C. Min, N. Chang, J. Cha, and J. Kang, "MIMO-OFDM downlink channel prediction for IEEE802.16e systems using Kalman filter," in *Proc. IEEE Wireless Commun. Netw. Conf.*, Mar. 2007, pp. 943–947.
[27] D. Tse and P. Viswanath, *Fundamentals of Wireless Communication*, Cambridge, U.K.: Cambridge Univ. Press, 2005.
[28] L. Huang, J. W. M. Bergmans, and F. M. J. Willems, "Low-complexity LMMSE-based MIMO-OFDM channel estimation via angle-domain processing," *IEEE Trans. Signal Process.*, vol. 55, no. 12, pp. 5668–5680, Dec. 2007.
[29] L. Huang, C. K. Ho, J. W. M. Bergmans, and F. M. J. Willems, "Pilot-aided angle-domain channel estimation techniques for MIMO-OFDM systems," *IEEE Trans. Veh. Technol.*, vol. 57, no. 2, pp. 906–920, Mar. 2008.
[30] A. M. Sayeed, "Deconstructing multiantenna fading channels," *IEEE Trans. Signal Process.*, vol. 50, no. 10, pp. 2563–2579, Oct. 2002.
[31] S. Kim, "Angle-domain frequency-selective sparse channel estimation for underwater MIMO-OFDM systems," *IEEE Commun. Lett.*, vol. 16, no. 5, pp. 685–687, May 2012.
[32] S. Zhou and G. B. Giannakis, "How accurate channel prediction needs to be for transmit-beamforming with adaptive modulation over Rayleigh MIMO channels?" *IEEE Trans. Wireless Commun.*, vol. 3, no. 4, pp. 1285–1294, Jul. 2004.
[33] S. Prakash and I. McLoughlin, "Effects of channel prediction for transmit antenna selection with maximal-ratio combining in rayleigh fading," *IEEE Trans. Veh. Technol.*, vol. 60, no. 6, pp. 2555–2568, Jul. 2011.
[34] R. O. Adeogun, P. D. Teal, and P. A. Dmochowski, "Extrapolation of MIMO mobile-to-mobile wireless channels using parametric-model-based prediction," *IEEE Trans. Veh. Technol.*, vol. 64, no. 10, pp. 4487–4498, Oct. 2015.
[35] A. Duel-Hallen, H. Hallen, and T.-S. Yang, "Long range prediction and reduced feedback for mobile radio adaptive OFDM systems," *IEEE Trans. Wireless Commun.*, vol. 5, no. 10, pp. 2723–2733, Oct. 2006.
[36] I. C. Wong, A. Forenza, R. W. Heath, Jr., and B. L. Evans, "Long range channel prediction for adaptive OFDM systems," in *Proc. Conf. Rec. 38th Asilomar Conf. Signals, Syst. Comput.*, Nov. 2004, pp. 732–736.
[37] J. Heo, Y. Wang, and K. Chang, "A novel two-step channel-prediction technique for supporting adaptive transmission in ofdm/fdd system," *IEEE Trans. Veh. Technol.*, vol. 57, no. 1, pp. 188–193, Jan. 2008.
[38] D. Schafhuber and G. Matz, "MMSE and adaptive prediction of time-varying channels for OFDM systems," *IEEE Trans. Wireless Commun.*, vol. 4, no. 2, pp. 593–602, Mar. 2005.
[39] L. Zhang, Z. Jin, W. Chen, and X. Zhang, "An improved adaptive channel prediction for MIMO-OFDM systems," in *Proc. 3rd Int. Conf. Commun. Netw. China*, Aug. 2008, pp. 1008–1012.
[40] J. Zhao, F. Gao, W. Jia, S. Zhang, S. Jin, and H. Lin, "Angle domain hybrid precoding and channel tracking for millimeter wave massive MIMO systems," *IEEE Trans. Wireless Commun.*, vol. 16, no. 10, pp. 6868–6880, Oct. 2017.
[41] D. Fan, Y. Liu, Y. Deng, and G. Wang, "Angle domain channel estimation in hybrid mmWave Massive MIMO systems," *IEEE Trans. Wireless Commun.*, to be published. [Online]. Available: https://www.researchgate.net/publication/328233208
[42] C. Lv, S. Hou, and W. Mei, "Adaptive prediction of channels with sparse features in OFDM systems," *Int. J. Antennas Propag.*, vol. 2013, 2013, Art. no. 649602.
[43] F. Wan, W.-P. Zhu, and M. N. S. Swamy, "A semiblind channel estimation approach for MIMO–OFDM systems," *IEEE Trans. Signal Process.*, vol. 56, no. 7, pp. 2821–2834, Jul. 2008.
[44] H. Minn and N. Al-Dhahir, "Optimal training signals for MIMO OFDM channel estimation," *IEEE Trans. Wireless Commun.*, vol. 5, no. 5, pp. 1158–1168, May 2006.
[45] P. S. R. Diniz, *Fundamentals of Adaptive Filtering*. Springer, 2013, ch. 2.
[46] J.-K. Hwang and J. H. Winters, "Sinusoidal modeling and prediction of fast fading processes," in *Proc. IEEE GLOBECOM*, Nov. 1998, pp. 892–897.
[47] J. B. Andersen, J. Jensen, S. H. Jensen, and F. Frederiksen, "Prediction of future fading based on past measurements," in *Proc. IEEE 50th Veh. Technol. Conf.*, Sep. 1999, pp. 151–155.
[48] *Study on Channel Model for Frequencies From 0.5 To 100 GHZ*, document Rec.3GPP TR 38.901 V15.0.0, Jun. 2018. [Online]. Available: http://www.3gpp.org/ftp/Specs/html-info/38901.htm
[49] W. Yuan, S. M. D. Armour, and A. Doufexi, "An efficient beam training technique for mmwave communication under nlos channel conditions," in *Proc. IEEE Wireless Commun. Netw. Conf.*, Apr. 2016, pp. 1–6.

[50] T. S. Rappaport, G. R. Maccartney, M. K. Samimi, and S. Sun, "Wideband millimeter-wave propagation measurements and channel models for future wireless communication system design," *IEEE Trans. Commun.*, vol. 63, no. 9, pp. 3029–3056, Sep. 2015.

CHANGWEI LV received the B.S.E. and Ph.D. degrees from the Beijing Institute of Technology, Beijing, China, in 2007 and 2015, respectively. From 2007 to 2009, he was a Research and Teaching Assistant with the Chongqing Information Institute, Chongqing, China. From 2015 to 2017, he was a Postdoctoral Research Associate with the Shenzhen Enterprise Postdoctoral Working Station, Shenzhen, China. He is currently a Lecturer with the Shenzhen Institute of Information Technology, Shenzhen. His research interests include signal processing and wireless mobile systems, with the emphasis on signal processing in wireless communications.

JIA-CHIN LIN (S'95–M'98–SM'03) received the Ph.D. degree in electrical engineering from the National Taiwan University, Taipei, Taiwan, in 1998.

He was in the obligatory military service, from 1998 to 2000, and then joined the Microelectronics and Information Systems Research Center, National Chiao Tung University, as a Research Assistant Professor. In 2001, he joined the Department of Electrical Engineering, National Chi Nan University, Taiwan, as an Assistant Professor. In 2004, he was promoted to the position of Associate Professor. In 2006, he joined the faculty of the Department of Communication Engineering, National Central University, Taiwan, as an Associate Professor. In 2008, he was promoted to the position of Full Professor. In 2011, he became a Distinguished Professor. He has also held visiting appointments at several universities, including Stanford University, Stanford, CA, USA, and Princeton University, Princeton, NJ, USA.

Dr. Lin received the Dr. Wu Da-You Research Award from the National Science Council, Executive Yuan, the Young Scientist Award issued by URSI, and the 2009 Ten Outstanding Young Persons Award of Taiwan. He has been serving as an Editor for the IEEE TRANSACTIONS ON VEHICULAR TECHNOLOGY, since 2008. He has been serving as a Technical Associate Editor for the *IEEE Communications Magazine*, from 2013. He has served as an Associate Editor for the IEEE SIGNAL PROCESSING LETTERS, from 2011 to 2012, and as a Guest Editor for the IEEE JOURNAL ON SELECTED AREAS IN COMMUNICATIONS (Special Issue on Emerging Technologies in Communications: Vehicular Networks and Telematics Applications.) He has also served as a Guest Editor for the *IEEE ITS Magazine*, and as a Guest Editor for the IET ITS.

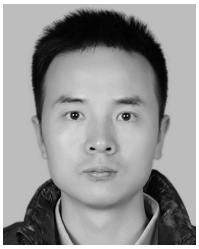

ZHAOCHENG YANG received the B.E. degree in information engineering from the Beijing Institute of Technology, Beijing, China, in 2007, and the Ph.D. degree in information and communication engineering from the National University of Defense Technology, Changsha, China, in 2013. From 2010 to 2011, he was a Visiting Scholar with the University of York, York, U.K. From 2013 to 2015, he was a Lecturer with the School of Electronics Science and Engineering, National University of Defense Technology. He is currently an Associate Professor with the College of Information Engineering, Shenzhen University, Shenzhen, China. His research interests include the area of signal processing, including array signal processing, adaptive signal processing, compressive sensing, and its applications to radar systems.